INTERANNUAL AND INTERDECADAL VARIABILITY IN UNITED STATES SURFACE-AIR TEMPERATURES, 1910–87 *

MICHAEL D. DETTINGER
U.S. Geological Survey, San Diego, California 92123–1135, U.S.A.; Department of Atmospheric Sciences and Institute of Geophysics and Planetary Physics, University of California, Los Angeles, California, U.S.A.

MICHAEL GHIL
Department of Atmospheric Sciences and Institute of Geophysics and Planetary Physics, University of California, Los Angeles, California, U.S.A.

and

CHRISTIAN L. KEPPENNE
Jet Propulsion Laboratory, California Institute of Technology/NASA, Pasadena, California 91109, U.S.A.

Abstract. Monthly mean surface-air temperatures at 870 sites in the contiguous United States were analyzed for interannual and interdecadal variability over the time interval 1910–87. The temperatures were analyzed spatially by empirical-orthogonal-function analysis and temporally by singular-spectrum analysis (SSA). The dominant modes of spatio-temporal variability are trends and non-periodic variations with time scales longer than 15 years, decadal-scale oscillations with periods of roughly 7 and 10 years, and interannual oscillations of 2.2 and 3.3 years. Together, these modes contribute about 18% of the slower-than-annual United States temperature variance. Two leading components roughly capture the mean hemispheric temperature trend and represent a long-term warming, largest in the southwest, accompanied by cooling of the domain's southeastern quadrant. The extremes of the 2.2-year interannual oscillation characterize temperature differences between the Northeastern and Southwestern States, whereas the 3.3-year cycle is present mostly in the Western States. The 7- to 10-year oscillations are much less regular and persistent than the interannual oscillations and characterize temperature differences between the western and interior sectors of the United States. These continental- or regional-scale temperature variations may be related to climatic variations with similar periodicities, either global or centered in other regions; such variations include quasi-biennial oscillations over the tropical Pacific or North Atlantic and quasi-triennial oscillations of North Pacific sea-surface temperatures.

1. Introduction

Atmospheric concentrations of carbon dioxide and other greenhouse gases are increasing and may approach twice their preindustrial values early in the next century (Watson *et al.*, 1990). Simultaneously, atmospheric concentrations of aerosols are increasing and may serve to counteract the greenhouse effect by reflecting and scattering solar insolation (e.g., Penner *et al.*, 1992). The individual and joint effects of these anthropogenic changes are unknown or, at least, uncertain. However, many climate researchers believe that global-scale changes in surface weather

Climatic Change **31:** 35–66, 1995.

will occur as a result of these upper-air changes, and that such changes already may be happening (IPCC Working Group I, 1992).

Detection of long-term trends in response to anthropogenic influences will depend on our ability to distinguish between natural and anthropogenic changes at global and regional scales, as well as between long-term change and short-term climate variability, and the reliability of these distinctions (Karl, 1988; Wigley and Barnett, 1990). Because natural climate variability occurs on all time scales, climate change is not readily ascertained using short records. For this reason, we must focus on the longest, cleanest, and most consistent climatic records available if we are to detect long-term climate change. Moreover, both long- and short-term climate variability will have to be quantified, if climate-change detection is to be reliable.

In this paper, long-term records of monthly mean air temperatures from the United States Historical Climatology Network (HCN: Karl *et al.*, 1990) are analyzed in terms of regional climate variability at interannual-to-interdecadal time scales. This data set was chosen for its length – 8 decades of broad regional coverage – and reliability, as it is arguably the most complete and uniform regional data set in the world (Karl and Quayle, 1988).

Although the contiguous United States – the region included in the HCN and considered here – covers only a small part of the Earth's surface, it is sufficiently large not to respond uniformly to global anthropogenic changes or natural climate variations. Consequently, the first step in our analysis is to describe the broad spatial aspects of historical United States temperature variations using spatial empirical-orthogonal-function (EOF) analysis, following Karl *et al.*'s (1982) approach. Temporal variability associated with the spatial temperature patterns so identified is then investigated by singular-spectrum analysis (SSA: Dettinger *et al.*, 1995) to single out the natural periodicities in the 2–20 year range.

The data and methods are described in Section 2. Results of the spatial analysis are discussed in Section 3, and are followed by a presentation of the major temporal modes of temperature variation in Section 4. Particular attention is given to the dominant low-frequency (LF) variations, i.e., nonoscillatory trends or long-periodic oscillations not captured reliably by the 78 years of record, and to oscillatory components (periodic or nearly periodic variations) present in the United States records. The latter components are the most regular and thus, presumably, most predictable natural variations in the interannual-to-interdecadal range. Oscillations are also most likely to be distinguishable from the one-time global and regional effects of our civilization. The major trends and oscillatory modes are compared with their counterparts in global- and hemispheric-mean temperatures during this century, to enable recognition of common modes of variability. Results are summarized and discussed in Section 5.

2. Data and Methods

Monthly mean temperatures from selected long-term sites in the HCN data set were deseasonalized, standardized, and gridded to ensure that variations throughout the contiguous United States received equivalent weightings in subsequent analyses. The gridded data set was then analyzed for its dominant spatial modes by spatial EOF analysis. In order to focus the full strength of the subsequent temporal analyses on interannual-to-interdecadal variability, the time variations of these spatial modes were filtered next to remove variations that are faster than annual, using various applications of univariate SSA. Finally, the spatio-temporal variability of the dominant spatial modes was analyzed for trends and oscillations using a multivariate form of SSA and several types of harmonic analysis. The methods used in each step are described in this section.

2.1. DATA SET

Monthly mean surface-air temperatures at 870 sites in the contiguous United States were extracted from the HCN data set (Karl *et al.*, 1990). The HCN data set includes records from 1,219 sites judged to be reasonably free from artificial changes in local environment over the duration of their record. Corrections for time-of-observation biases, station movement, and local urbanization effects have been applied and are described by Karl *et al.* (1990).

The 870 sites used in this study, which are shown in Figure 1(a), were chosen for their serial completeness between 1910 and 1987. Before about 1910, the geographic coverage of the network drops rapidly in the Western States.

2.2. DATA PREPARATION

In anticipation of the temporal analyses to follow, the monthly mean temperatures at each site were standardized by subtracting from each set of monthly (January to December) values the 78-year mean-monthly temperature for that month and dividing the difference by the corresponding long-term monthly standard deviation. That is, for each site and month, we formed the temperature index:

$$\overline{T}(i,\ j,\ k) = [T(i,\ j,\ k) - T_{\mathrm{M}}(i,\ k)]/\sigma_T(i,\ k)\ . \tag{1}$$

In (1), $T(i,\ j,\ k)$ is the HCN value of mean temperature at site k during month i of year j, $T_{\mathrm{M}}(i,\ k)$ is the mean-monthly temperature at site k for month i, and $\sigma_T(i,\ k)$ is the standard deviation of $T(i,\ j,\ k)$ from $T_{\mathrm{M}}(i,\ k)$.

Subtracting the mean-monthly normals removes much of the annual cycle at each site. Dividing by the monthly standard deviations removes still more seasonality and prevents the sites with more variability from overwhelming their surroundings in the covariance analyses to follow. The analysis was also carried out with the temperatures having the mean seasonal cycle removed, but not being

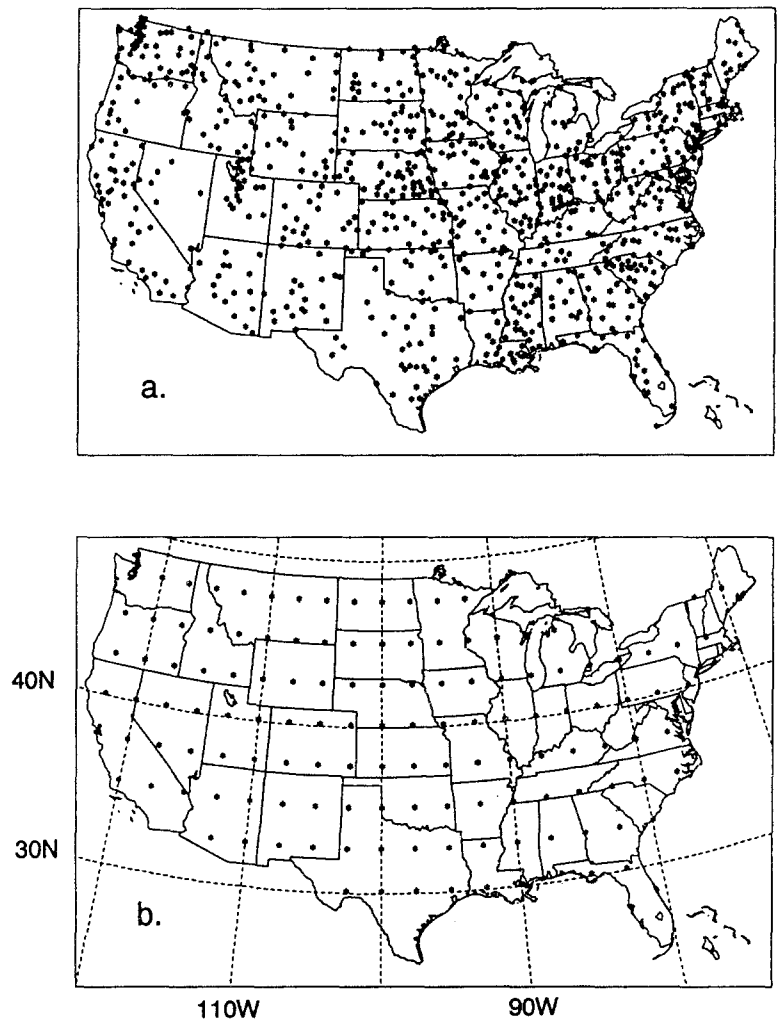

Fig. 1. Locations of (a) Historical-Climatology Network (HCN) sites with serially complete surface-air temperature records since 1910; and (b) 2.5°-by-2.5° grid points.

normalized. Neither this nor a number of other methods of data preparation had a substantial effect on the results. The seasonal cycle must be removed because an extremely strong periodic component can overwhelm SSA and hamper its ability to capture some of the remaining oscillations.

In order to prevent the regions that have more HCN sites from dominating the spatial patterns (Karl *et al.*, 1982; North *et al.*, 1982), the temperature indices $\overline{T}(i,\ j,\ k)$ were interpolated onto a rectangular 2.5° latitude by 2.5° longitude grid of $N_G = 131$ points (Figure 1b) using the 'optimal interpolation' method of Yamamoto and Hoshiai (1980). This grid is four times as dense as the global $5° \times 5°$ grid of Jones *et al.* (1986a, b), and the data set chosen (1910–87) provides

one or more HCN observations each month within a 250-km radius of each grid point.

The optimal interpolation was performed assuming that the natural variability of the surface-air temperatures is described by a homogeneous, isotropic Gaussian correlation structure and – arbitrarily – that the spatial decorrelation distance of the combined measurement and sampling errors (Lorenc *et al.*, 1991) is only 150 km (see, however, Handcock and Wallis, 1994, for a more advanced random field model). This small decorrelation distance ensured that the gridded values remain close to the immediately surrounding temperature observations. The resulting gridded temperatures have an approximately Gaussian spatial correlation structure but with a correlation distance of roughly 1,700 km, in good agreement with distances of 1,500–2,000 km estimated for gridded temperatures over larger regions (Madden *et al.*, 1993; Mann and Park, 1994). Use of one of these larger correlation distances for the error structure would have *imposed* a large correlation distance and a very small number of spatial degrees-of-freedom (*d-o-f*) on the gridded data set; notice, for example, that the entire grid is only about $3,500 \times 1,700$ km or about 2×1 of these correlation distances. It will be shown in Section 3 that the gridded data set contains about 5 *d-o-f*. By assuming a small correlation distance in the interpolation process, we are confident that this small number of *d-o-f* is inherited from the observations rather than the interpolation. To check the sensitivity of the analyses that follow to the gridding method and interpolation assumptions, temperature indices were also interpolated as weighted averages of temperatures at the nearest three sites in each quadrant surrounding the grid point (Ghil *et al.*, 1979). The resulting gridded temperature indices and their spatial EOFs were similar to those obtained using optimal interpolation.

2.3. SPATIAL EOF (S-EOF) ANALYSIS

The gridded temperature indices were analyzed to determine the dominant spatial modes of variability by S-EOF analysis (Preisendorfer, 1988), a variant of principal-component (PC) analysis applied to spatially distributed functions. The resulting S-EOFs are normalized eigenvectors of the sample spatial-covariance matrix. That is, they are the solutions to:

$$Re_l = \lambda_l e_l \,, \tag{2}$$

in which R is the N_G-by-N_G sample spatial-covariance matrix between all pairs of temperature indices $\overline{T}(i,\ j,\ k)$ among the N_G-grid points, e_l are its eigenvectors normalized to unit length, and λ_l is the eigenvalue corresponding to e_l. Thus defined, the S-EOFs are orthonormal data-adaptive patterns $e_l = e_l(k)$ that capture the maximum fraction of the temporal and spatial variability of the temperature indices in the fewest (nondimensional) 'maps'. The temporal variability that each

S-EOF represents is accounted for by the corresponding spatial PC (S-PC), a time series $a_l = a_l(i,\ j)$ defined by:

$$a_l = \mathrm{Z}e_l\ , \tag{3}$$

where a_l is the S-PC associated with the l-th S-EOF, and Z is an $N_T \times N_G$ matrix of $\overline{T}(i,\ j,\ k)$, where $N_T = 936$ is the total number of months of observations.

Part or all of the original series of maps can be reconstructed from the complete set of S-EOFs and S-PCs according to:

$$Z' = A'E', \tag{4}$$

where A' is the matrix with columns equal to selected a_l's, and E' is the matrix with columns equal to the corresponding e_l's. If E' and A' contain all N_G of the S-EOFs and S-PCs, respectively, the original maps are reconstructed in their entirety, Z' = Z. If only the L' leading S-EOFs are summed, then only the most important part of the original variability is reconstructed. Various criteria have been proposed to judge how many S-EOFs must be discarded to eliminate noise in subsequent analyses. In Section 3, attention is restricted to a few large-scale patterns that capture most of the temperature variability, on the basis of Guttman's (1954) lower bound on the significance of EOFs (see Figure 2 below for definition) and on the basis of detection of a prominent break in the spectrum of eigenvalues (to be described later).

2.4. SINGULAR-SPECTRUM ANALYSIS (SSA)

In order to focus later analyses more directly on the interannual and interdecadal time scales, selected S-PC series were prefiltered to remove variability faster than annual before being analyzed for longer term trends and oscillations. SSA (Colebrook, 1978; Broomhead and King, 1986; Fraedrich, 1986; Vautard and Ghil, 1989; Ghil and Vautard, 1991; Vautard *et al.*, 1992) – a form of temporal PC or EOF analysis – was used for both prefiltering and the long-term analysis of the filtered time series. SSA is a powerful form of PC analysis of the lag-correlation structure of time series (Vautard *et al.*, 1992; Dettinger *et al.*, 1995) that is particularly successful in isolating multiple periodic components and trends in short, noisy series. SSA has been applied to univariate time series (e.g., Ghil and Mo, 1991a, b; Keppenne and Ghil, 1992; Plaut *et al.*, 1995), to spatially correlated series (Kimoto *et al.*, 1991; Keppene and Ghil, 1993; Plaut and Vautard, 1994), and, in this study, to uncorrelated series.

In univariate SSA, the eigenvectors of the lag-correlation matrix of a single time series, referred to as temporal EOFs (T-EOFs), provide the basis functions that most efficiently describe the time series. By analogy with S-EOF analysis, the strengths of these patterns are described by temporal PCs.

In multivariate SSA (M-SSA: Weare and Nasstrom, 1982; Lau and Chan, 1985; Kimoto *et al.*, 1991), the EOFs are normalized eigenvectors of a block [$M \times C$-by-$M \times C$] lag-cross-correlation matrix between C time series – or channels, such as

the leading S-PCs of the preceding S-EOF analysis – with lags ranging from 1 to M times Δt, the sampling interval. The EOFs in M-SSA contain elements of both spatial and temporal variability and are called space-time EOFs (ST-EOFs: Plaut and Vautard, 1994). The correlation matrix is estimated, *cf.* Equation (2.3) of Vautard *et al.* (1992), so that it has block Toeplitz structure with $C \times C$ blocks. This approach imposes symmetry (or antisymmetry) around the mid-lag point upon the resulting ST-EOFs, and in the present application seems to yield 'cleaner' decompositions of the spatio-temporal temperature variability than the non-Toeplitz approach of Broomhead and King (1986). Allen (1992) has found that this Toeplitz structure yields stabler T-EOF patterns but that it may induce flattening of SSA trends at the ends of the time series. Space-time PCs (ST-PCs) are obtained from a temporal counterpart to (3), and are still time series; the ST-EOFs are, when $C \geq 2$, sequences of M (suitably normalized) 'maps'. As in (4), all or part of the original time series can be reconstructed from the ST-EOFs and ST-PCs for all or part of the M available pairs of scalar or vector 'points' in the time series. For convenience, we have rescaled the ST-EOF segments corresponding to each S-PC by the standard deviations of the original S-PC series.

If long-term variations – including trends – are present in the time series being analyzed, one or two T-EOFs or ST-EOFs typically capture those variations that repeat themselves only at periods greater than the maximum lag considered or not at all (Ghil and Vautard, 1991; Unal and Ghil, 1995). This property was used to filter the leading S-PCs to remove variations that are faster than annual in a data-adaptive manner, without reducing the sampling interval. If discrete annual values had been used instead – to avoid this filtering step – interannual oscillations in the 2–3 year range would not have been resolved in the subsequent M-SSA. Immediately following S-EOF analysis, each leading S-PC was subjected to univariate SSA with a window of 12 months. T-EOFs that capture variations slower than the window width are of uniform sign or show only one sign change. By counting the number of zero crossings in each of the 12 T-EOFs, in each case, the two T-EOFs that contained most of the variability slower than the 12-month window were identified, and just that part of the overall temperature variations was reconstructed according to (4). By this method, each S-PC series was stripped of faster-than-annual variability.

SSA responds to oscillatory components by forming pairs of T-EOFs or ST-EOFs, with each pair filtering adaptively for one or two of the dominant frequencies present (Vautard and Ghil, 1989). In M-SSA, these oscillations may span all or some of the time series considered. Previous studies have shown that SSA is successful at reliably isolating even weak oscillations in short, noisy climatic series (e.g., Rasmusson *et al.*, 1990; Penland *et al.*, 1991; Keppenne and Ghil, 1992). A pair of oscillatory ST-EOFs and their ST-PCs are in quadrature with each other (Ghil and Mo, 1991a, b), thus facilitating the visualization of the oscillation's main phases. Consequently the ST-EOFs often take the form of simple sine-cosine pairs for each channel at the frequency captured.

The pairs may be identified tentatively by their nearly equal eigenvalues (Vautard and Ghil, 1989). Several tests were performed to document the oscillatory nature and quadrature relations of pairs of ST-EOFs suspected to representing periodicities in the time series. First, the power spectra of the ST-PCs were determined. If the ST-PCs were strongly concentrated in just a few frequencies and if the two ST-PCs shared the same frequencies, then the pair was suspected of representing a single periodic oscillation (see Vautard *et al.*, 1992). The ST-PCs corresponding to apparently periodic ST-EOFs were tested for quadrature by estimating the lags at which cross-correlations were maximized (Ghil and Mo, 1991a, b). These cross-correlation maxima were compared with the range of correlations at the same lags in surrogate ST-PCs obtained from red-noise realizations (of first-order autoregressive processes). The surrogate ST-PCs were generated by projecting 1,000 red-noise series (with the same length, number of channels, observed variance, and lag-one correlations as the real S-PCs) onto the suspected oscillatory ST-EOFs, following loosely the fixed-bases approach to significance testing of Allen and Smith (1994). If the lag-cross-correlations in Table I (see Section 4) exceed (in magnitude) those of 95% of the surrogate ST-PCs, the correlations are judged to reflect significant signals. If the significant cross correlations are found for lags equal to one quarter of the apparent period of the ST-EOFs, then the components are judged to be in quadrature.

2.5. HARMONIC ANALYSIS

Because SSA is data-adaptive, it yields T-EOFs or ST-EOFs precisely fitted to isolate the significant oscillations in a series directly rather than by exhaustively searching all frequencies. Therefore, no direct frequency estimate for the oscillatory components is provided and some form of harmonic analysis must be applied to them in order to precisely determine their periodicities. In this study, the maximum entropy method (MEM) of spectrum analysis (Burg, 1978; Press *et al.*, 1989) was applied to determine peak frequencies in selected SSA components. This method provides high-resolution spectral estimates, but it can yield spurious peaks. Penland *et al.* (1991) have shown that SSA prefiltering can eliminate the spurious peaks, while maintaining the high resolution of MEM. To further corroborate the spectral peaks found by MEM, the multi-taper method (Thomson, 1982) and Blackman-Tukey method (Kay, 1988) were also applied.

MEM spectra of grid-point and regional-mean reconstructions of leading temperature oscillations were also computed. These spectra (Figure 7 in Section 4.1.) confirm the precision with which the combination of M-SSA and MEM extracts individual harmonics from otherwise broad and noisy spectra. The MEM spectra also suggest two limitations that impede spatio-temporal analyses by MEM of regional or S-EOF patterns: Although spectra of series from different regions can illustrate relative strengths of oscillations in those regions, they contain no information about either the phase relations among the regions or time variations of

the amplitudes of the oscillations. M-SSA together with harmonic analysis retains these relations even as it provides powerful data-adaptive filtering to isolate the oscillations.

3. Spatial Analysis of United States Temperatures

3.1. BI-ORTHOGONAL EOFS

S-EOF analysis was applied to the gridded temperature-index record, first without rotation; rotated EOFs are considered in Section 3.2. The log-eigenvalue spectrum of the unrotated, bi-orthogonal S-EOFs is shown in Figure 2. The nine leading S-EOFs contribute a greater percentage of the temperature variability than Guttman's (1954) lower bound on EOF significance, which is indicated by horizontal lines in Figures 2a and 2b. The lower bound is the percentage of variance that would be contributed by the EOFs of completely white (uncorrelated) noise on a grid of the same size. In nature, white noise is less common than red or 'colored' noise (Ghil and Childress, 1987); the latter is broadly enriched in low frequencies. Thus, the significance of leading EOFs is commonly judged not just by their contributions relative to Guttman's lower bound but also by their contributions relative to the shallow sloping ramp of log-eigenvalue, $\log\lambda_l$, against order l that starts roughly near the $l = 20$ (in Figure 2b).

In a spatially coarser analysis, Karl *et al.* (1982) analyzed mean winter temperatures averaged by state and captured roughly 90% of winter variance with their leading three S-EOFs. As shown in Figures 2a and 2b, however, five S-EOFs in the present study plot above both the break in slope and the level of the red-noise ramp in the spectrum. Notably, the gap between the eigenvalues for EOFs 5 and 6 is three times the *ad hoc* estimate of eigenvalue sampling error (following North *et al.*, 1982) whereas there is no gap between the error bars of the higher-order eigenvalues, including the noise background. Consequently, the remainder of this analysis focuses on the first five S-EOFs, which together contribute 84% of the variance in the gridded monthly HCN temperatures.

There are thus, roughly, five spatial *d-o-f* in the monthly HCN temperature data set. The $2.5° \times 2.5°$ gridding permits, on the one hand, a detailed description of the spatial *d-o-f*, and it provides, on the other, increased confidence that this low number of spatial *d-o-f* is not an artifact of crude data preparation (see Section 2.2. above).

The five leading S-EOFs are mapped in Figure 3. The first S-EOF is positive everywhere, with highest values in the north-central states. This S-EOF and its S-PC capture the 38% of temperature variability that is simultaneous over the entire grid. Notice that the central, continental region varies more than the coastal regions in this mode, in spite of the normalization of the temperature indices by local standard deviations.

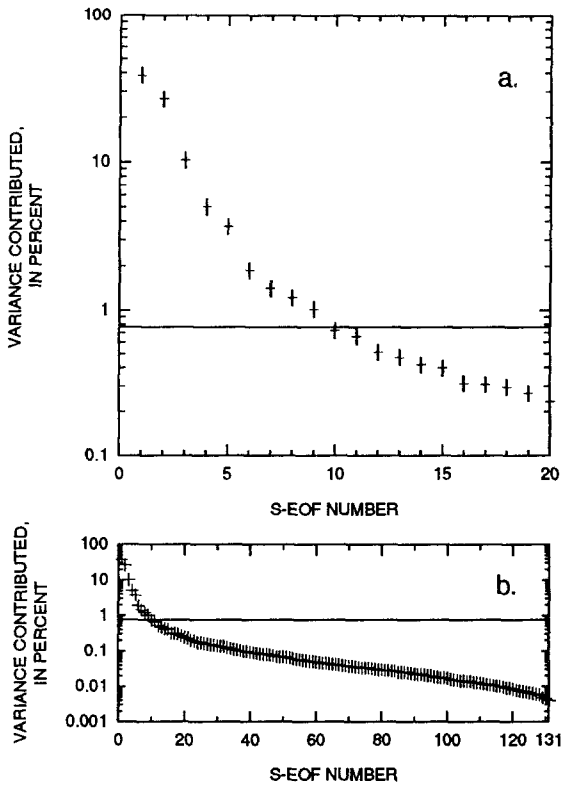

Fig. 2. Variance contributed by spatial PCs and spatial EOFs (S-EOFs) of gridded HCN monthly temperature indices, 1910–87: (a) Leading 20 eigenvalues; and (b) all $N_G = 131$ eigenvalues; horizontal lines indicate Guttman's (1954) lower bound ($100/N_G$). Vertical error bars are based on the *ad hoc* estimate proposed by North *et al.* (1982) – $\lambda(2/N_G)^{1/2}$ – where λ is the eigenvalue estimate.

The second S-EOF represents east-west temperature differences, and contributes 27% of the overall variance. The third S-EOF (10% of variance) represents north-south temperature differences. S-EOF 4 captures temperature differences between the central and coastal regions, and S-EOF 5 temperature variations in which the Northwest and Southeast vary in opposition to the Southwest and Northeast.

S-EOFs 4 and 5 contribute 5.0 and 3.7% of the temperature variance, respectively, and thus differ by only 1.3%. This difference is comparable to their combined *ad hoc* estimated error bars of about 1.1%. Thus, the eigenvalues for these two S-EOFs are close to degeneracy (Press *et al.*, 1989). As a result, the corresponding S-EOF patterns may not be unique, and linear combinations of these S-EOFs may also emerge as valid S-EOFs if the raw data set or its preparation were perturbed but slightly. Also, the simple patterns – whole-domain, east-west, north-south, and so on – described by the S-EOFs are more suggestive of variance maximization, subject to orthogonality constraints, in a rectangular domain (Richman, 1986) than of distinct physical processes. We consider, therefore, in the next subsection, rota-

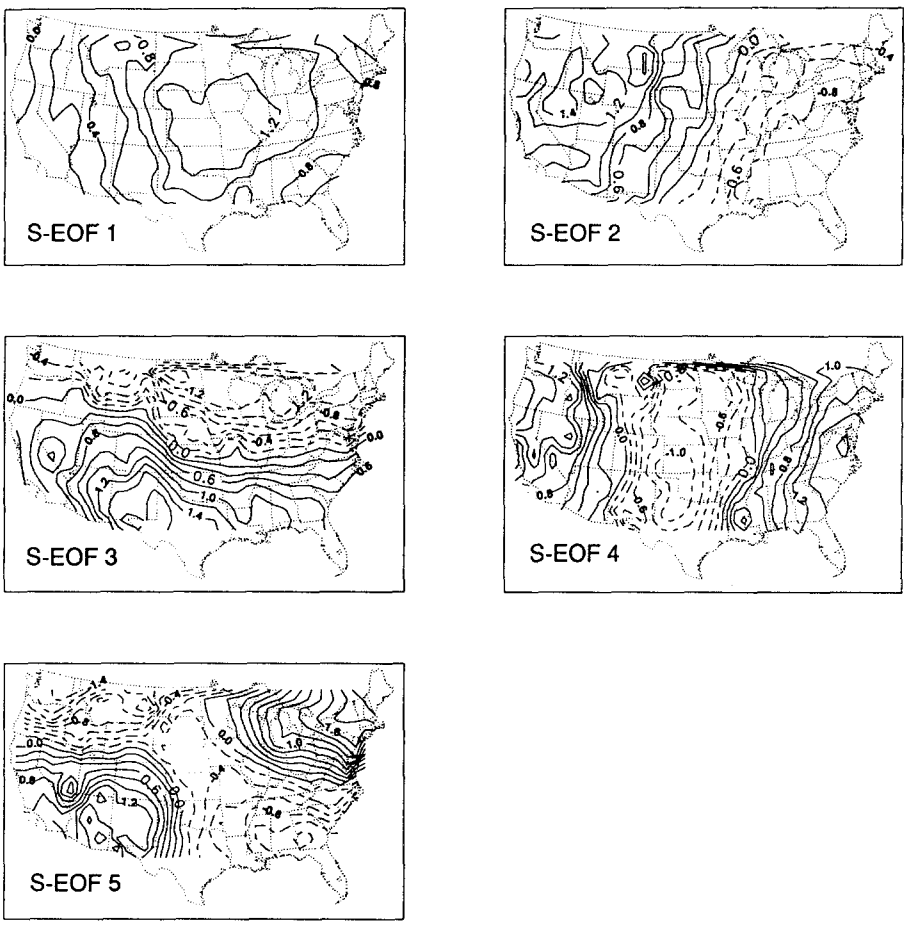

Fig. 3. Leading S-EOFs of gridded temperature indices; normalized to unit-vector length, times 10. Contour interval is 0.2; dashed where negative.

tion of the S-EOFs, a procedure commonly used to reduce pattern indeterminacy and spatial-domain dependence. It turns out that M-SSA offers a more consistent spatio-temporal description of the temperature variations and that, in the final analysis, the bi-orthogonal, unrotated EOFs are more parsimonious in terms of describing spatio-temporal variability via M-SSA. When M-SSA – which provides a simultaneous analysis of all five S-PCs – is used, S-EOFs 4 and 5 can be treated simultaneously without requiring individual attention or common rotation. Furthermore, with M-SSA, the leading S-PCs are analyzed simultaneously and the simple near-rectangular S-EOF patterns are not interpreted as distinct processes. The reader less interested in technical details may therefore skip Section 3.2. or return to it at a later time.

Filtered S-PC series for the five leading (unrotated) S-EOFs are shown in Figure 4. Each S-PC was filtered by application of univariate SSA with a 12-month

window followed by reconstruction of the slower-than-annual SSA components. All five filtered S-PC series contain considerable interannual variability; much of this appears to be periodic, at least intermittently. In addition, S-PCs 1, 2, 4, and 5 show slow variations that have periods comparable to the 78-year record considered, or longer trends. Together, these five filtered S-PCs contribute the slowest 18 percent of the total temperature-index variability. Their interannual and interdecadal variations are studied in detail in Section 4.

3.2. ROTATED EOFS

To remove indeterminacies, S-EOFs can be further constrained by a form of cluster analysis that *rotates* the patterns to maximize their differences. The S-EOFs analyzed by M-SSA later in this study are unrotated, as in Section 3.1. above, and describe the maximum fraction of temporal and spatial variability of the temperature indices in the fewest spatial patterns (Richman, 1986). They could be, and appear to be, influenced by the generally rectangular spatial domain of the gridded data (e.g., Legates, 1991, 1993; Richman, 1993). Such influence typically results in S-EOFs that are simple rectangular subdivisions of the rectangular domain, with progressively smaller subregions of uniform sign as the S-EOF number increases.

Thus, the S-EOF patterns probably are oversimplifications of the true modes of spatial variability and do not represent individually the influence of distinct physical processes (Ghil and Mo, 1991a, b). The goal here, however, is not to identify each individual S-EOF with a separate process, but rather to identify large-scale spatio-temporal trends and oscillations. These variations can be represented by either rotated or unrotated S-EOFs as long as the leading EOFs are analyzed simultaneously. For the sake of completeness, however, the first five S-EOFs were rotated orthogonally by the Varimax method (Richman, 1986). The rotated S-EOFs (not shown) divide the grid into north-central, northwestern, southwestern, southeastern, and northeastern regions. The corresponding rotated S-PCs individually include oscillations with virtually the same periodicities as those found in the M-SSA based on unrotated S-PCs below. Where useful, these rotated patterns will be mentioned in the following sections. The same leading periodicities were also recovered when only three S-EOFs were retained in the M-SSA (following Karl *et al.*, 1982), but the spatio-temporal oscillations could not be separated from each other in this artificially restricted analysis.

Ultimately, the large-scale picture of interannual and interdecadal oscillations that was sought can be obtained from either the S-EOFs (rotated or not) – by summing them up to the scale of the patterns shown in Figure 3 and accounting for the phase differences between oscillations in the various S-PCs – or, alternatively, by applying M-SSA. In most of this study, we focus on an M-SSA of the unrotated S-EOFs. This choice involves no loss of discrimination because the same overall variability is captured by the rotated and unrotated representations of the temper-

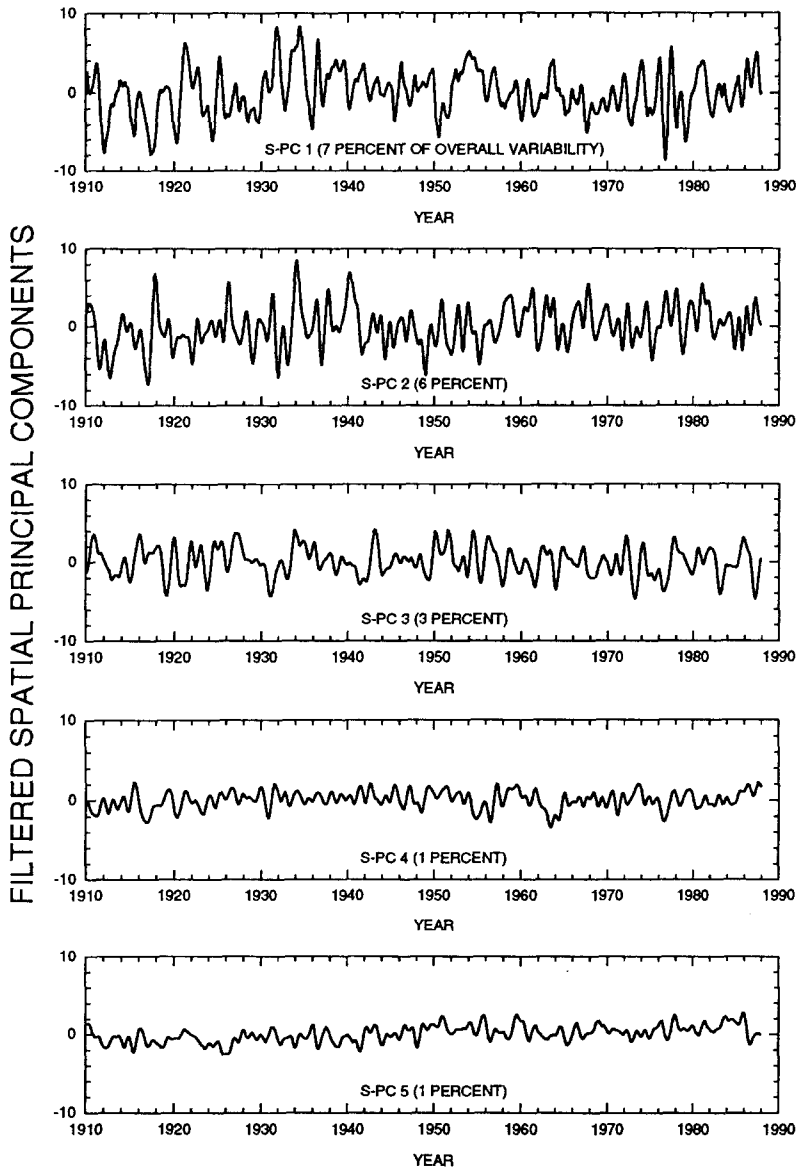

Fig. 4. Filtered spatial PC (S-PC) series for the five leading S-EOFs of gridded temperature indices. The series contribute the percentages of overall (unfiltered) temperature-index variability shown.

ature indices, and M-SSA addresses that overall variance rather than the variance in each S-EOF separately. The indeterminacies of the fourth and fifth S-EOFs, and the likelihood that the individual S-EOFs inherit their shapes from the shape of the domain, present no more of a problem in this application of M-SSA than they would in a rotated S-EOF analysis. Indeed, the rotated S-PCs were collectively analyzed by M-SSA and showed the same oscillations and trends. In this case, however, the

spatial patterns of the oscillations at various frequencies could not be reconstructed separately. Thus, M-SSA of unrotated S-PCs gave a clearer description of the various oscillatory patterns in the United States temperature record.

Finally, in order to test the robustness of these spatial results, the same analyses were carried out for (1) a similarly gridded set of centered but not standardized temperatures (as mentioned previously, in Section 2.2.); and (2) a version of the temperature-index data that was prefiltered for subannual frequencies separately at each grid point, prior to determination of S-EOFs. Similar S-EOF patterns, S-PCs, and oscillations were obtained from the centered temperatures, except where the indeterminacy of S-EOFs 4 and 5 interfered. For example, all the filtered S-PC series were correlated to corresponding components in the present analysis at 0.90 levels and greater (except for S-EOFs 4 and 5 of analysis (1) above). The results below are thus largely insensitive to data preprocessing.

4. Spatio-Temporal Analysis of United States Temperatures

The five filtered S-PC series shown in Figure 4 were subjected to M-SSA using a window size of 15 years and quarterly mean S-PC values. Because of the filtering already applied, this quarterly sampling was observed to reduce the computational burden without altering the results to follow. The analysis yielded the eigenvalue spectrum shown in Figure 5(a), which illustrates the relative contributions of the leading M-SSA components to the temperature variability of the five S-PCs. Error bars for the variance contributions shown in Figure 5 are based on a modification of the *ad hoc* estimates of uncertainty used in Ghil and Mo (1991a) and Vautard and Ghil (1989). Error bars were estimated by:

$$\delta\lambda_k = (2\tau/N_T)^{1/2}\lambda_k \,, \tag{5}$$

where τ is a typical decorrelation time (Unal and Ghil, 1995; equal here to one year, within which lag correlations declined to 1/e in all five S-PC series), and N_T is the number of quarterly values. The error estimate (5) is less conservative than the Ghil and Mo (1991a) estimate, $\delta\lambda_k = (2M/N)^{1/2}\lambda_k$, and more conservative than that used by Vautard and Ghil (1989), $\delta\lambda_k = (2/N)^{1/2}\lambda_k$. On the basis of these error bars, the first three M-SSA components contribute substantially more variance, and the next eight marginally more variance, than is extrapolated from the red-noise background of the remaining components (Figure 5(b)).

A more refined significance test was made by comparing the variance contributed by each of the first 11 components to that contributed by the same patterns (ST-EOFs) in 1,000 red-noise realizations with the same length, number of channels, variances, and lag-one correlations as in the real S-PCs. Each of the realizations was projected onto each of the first 11 ST-EOFs to estimate the variance that these patterns would be expected to capture from red noise, in an abbreviated form of the fixed-basis test proposed by Allen and Smith (1994). Those ST-EOFs that capture

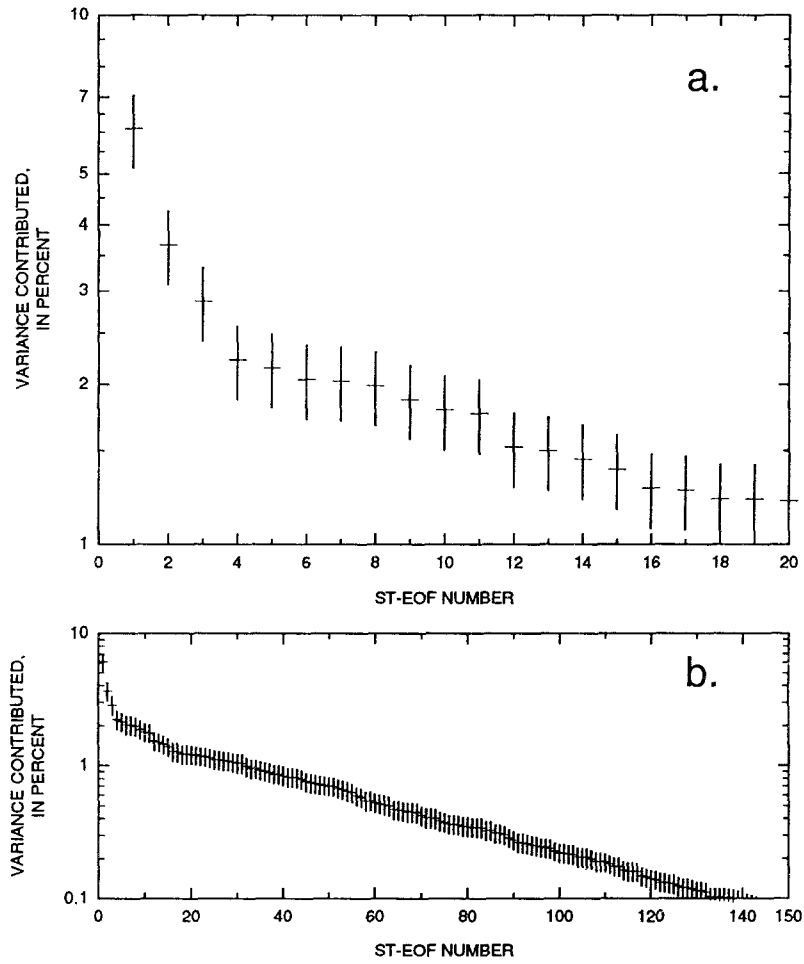

Fig. 5. Variance contributed to the five leading S-PCs of United States temperature indices, as captured by multivariate SSA (M-SSA), (a) for 20 leading space-time EOFs (ST-EOFs); and (b) for 150 leading ST-EOFs. Error bars described in text (see Equation 5).

more variance than 95 percent of the red-noise surrogates are indicated in Table I. Among the 11 components tested, the third component cannot be distinguished from the surrogates, at this level. The fourth and fifth components are marginally significant (within a percent or two of 95% confidence levels), whereas the eighth and ninth components do not pass the 95% confidence test but do pass a 90% test. Components 1, 2, 6, 7, 10, and 11 pass 95% confidence tests easily. All the leading components easily pass similar tests based on white-noise surrogates (processes with no autocorrelations).

A search of the 11 leading ST-EOFs showed that some pairs are representative of oscillations in the temperature records. As shown in Table I, ST-PCs 4–5, 6–7, 8–9,

TABLE I

Variance contributions, dominant periodicities, and lag cross-correlations from leading low-frequency and oscillatory components of United States temperature indices, 1910–87. Variance contribution is percentage relative to total slower-than-annual variability; highlighted where significant at 95% level in comparisons with 1,000 red-noise series. (Variance contributed by components 4–5 is very nearly significant at 95% level.) Similarly, correlations are highlighted where significantly different from red-noise correlations.

Component (ST-EOF number)	Variance contributed (percent)	Dominant periodicity (cycles/year)	Maxima of lag cross correlations
1	**4.9**	*	–
2	**3.0**	*	–
3	2.3	*, minor power at 7.7	–
4–5	3.5	10 and 7.4	+ **0.91** at 24 months – **0.78** at 75 months
6–7	**3.3**	2.2	+ **0.93** at 6 months – **0.91** at 21 months
8–9	3.1	6.7	– **0.88** at 6 months + 0.68 at 21 months – 0.58 at 75 months
10–11	**2.9**	3.3 and 4.0	– **0.93** at 9 months + 0.80 at 30 months

* Trend, or period longer than 15-year window.

and 10–11 constitute relatively simple signals (only one or two dominant periodicities). Components 4–5, 6–7, and 10–11 also yield significant lag-correlations at about one-quarter period (in comparison with the red-noise surrogates). No 'pure' oscillatory pairs were found among ST-PCs 12–20; instead, each of these ST-PCs was a complicated (but weak) mix of the dominant frequencies found in the leading components (mixing periodicities of roughly 2, 3, and 10 years).

On the basis of these considerations, only M-SSA components 1, 2, 4–5, 6–7, and 10–11 will be addressed in detail. Together, these components contribute 18% of the slower-than-annual temperature-index variability. Components 1 and 2 represent significant LF variability. Although each of components 4–11 contributes individually but slightly more variability than the red-noise slope, the oscillations that they capture in the United States temperature record are confirmed by several univariate and multivariate SSA analyses of either rotated or unrotated S-PCs using window widths of 10 years (Keppenne *et al.*, 1994), 15 years (presented here), or 25 years (Dettinger and Ghil, 1992). Each of the oscillatory pairs considered here (except possibly 8–9) appears to be significantly different from the noisy back-

ground. The LF variations, interannual oscillations, and then the more irregular, longer-term oscillations will be discussed in turn.

4.1. LOW-FREQUENCY (LF) VARIABILITY

LF variability (see Section 1) is defined as capturing (nonlinear) trends and oscillations with periods longer than the window width of 15 years. M-SSA components 1 and 2 represent distinct forms of LF variability. Shown in Figure 6 are ST-EOFs 1 and 2 (panels (a)–(b)) and ST-PCs 1 and 2 (panel (c)). To ease comparisons with other time series, the ST-PCs are plotted according to the midpoints of the windows. Because the five channels of the ST-EOFs have been weighted by the standard deviations of the corresponding S-PCs prior to plotting, the relative contributions of each S-PC can be read directly from Figures 6(a), (b).

ST-EOF 1 and ST-PC 1 provide the simplest example of how to interpret ST-EOFs and ST-PCs in M-SSA. As shown in Figure 6(a), for the variability captured by ST-EOF 1, each S-PC obtained from a filter that is symmetrical with respect to lag – the corresponding column of the ST-EOF. The filters for S-PCs 1, 3, and 4 have small positive weights. In contrast, the weights for S-PCs 2 and 5 are negative and two-to-three times larger in magnitude. The combined filter responses of the five S-PCs form a single declining ST-PC series (solid curve in Figure 6(c); notice that abscissa is reversed for comparison to temperatures). Together with the negative weightings in the ST-EOF, this steady ST-PC decline is translated mostly into a gradual temperature increase in those regions that have positive values of S-EOFs 2 and 5 (Figures 3(b) and 3(e)), and temperature decreases where these values are negative. The positive and negative weights in S-EOFs 2 and 5 reinforce each other in the southwest and southeast quadrants of the domain but cancel each other in the northwest and northeast quadrants. As a result, ST-PC 1 mostly describes a gradual cooling in the southeast and a smaller warming in the southwest quadrants during the 78 years of record studied here. This almost monotonic trend is fairly robust to procedural variations, including rotation of the S-EOFs.

The second M-SSA component is also dominated by variations on time scales comparable to the 78-year length of record (dashed curve in Figure 6(c)), but it is not as monotonic as ST-PC 1. ST-PC 2 is mostly weighted on S-PC 1 (the whole-domain pattern), cf. Figure 6(b); thus it is not surprising that its variation roughly parallels the LF variation of the United States average-temperature series (Figure 6(d)). Reconstructions of ST-PC 2 variability indicate an enhancement of the signal in the Southeastern United States. Interestingly, ST-PC 2 also resembles the LF components of the Northern Hemisphere (NH) mean temperature series (dotted line in Figure 6(d)) which, in turn, follows trends in sea-surface temperature in the North Equatorial Atlantic Ocean (Allen and Smith, 1994), nearest the Southeastern States.

The separation of the five S-PCs into LF variations and shorter-term oscillations by M-SSA is illustrated in the MEM stack spectra of Figure 7. The curves in each

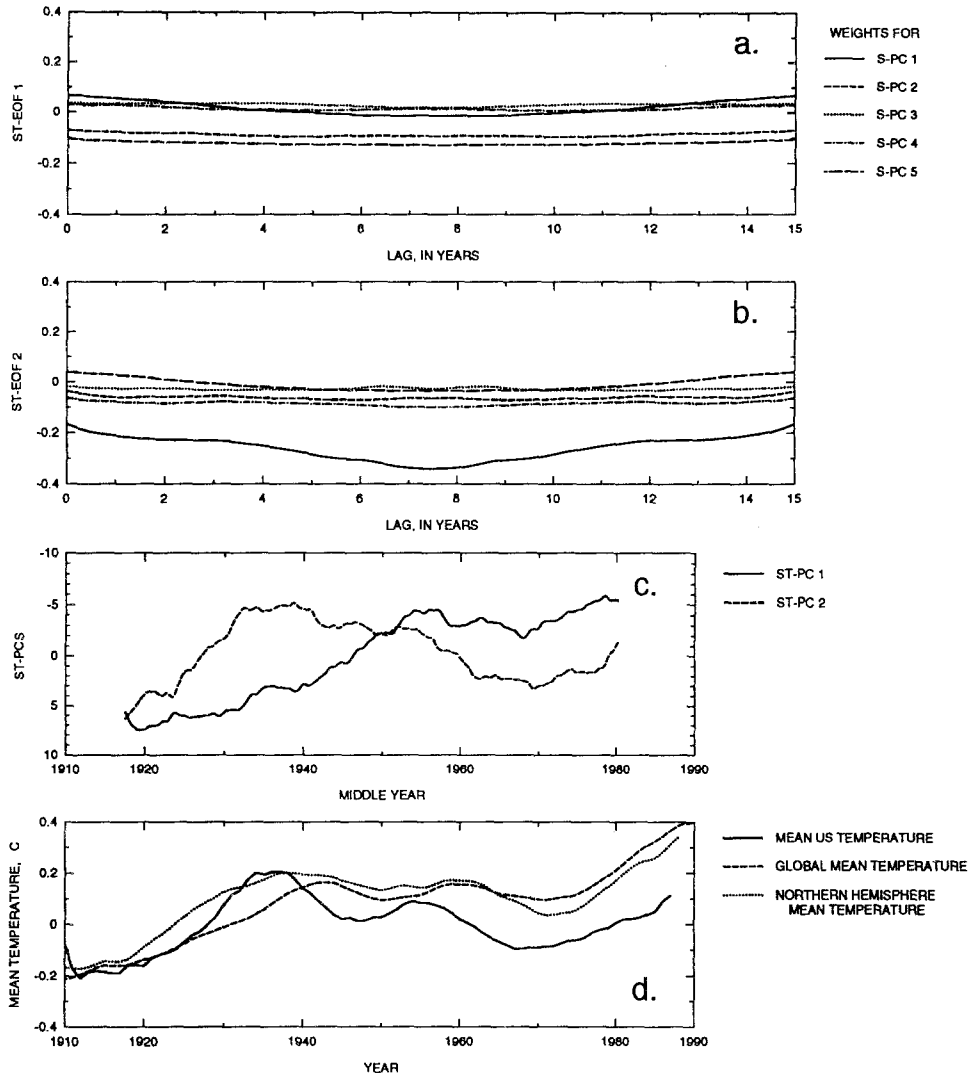

Fig. 6. Space-time EOF (ST-EOF) weightings and space-time PCs (ST-PCs) for M-SSA components 1 and 2, and some large-scale climatic indices: (a) ST-EOF weights, component 1; (b) ST-EOF weights, component 2; (c) ST-PCs for components 1–2; and (d) global- (IPCC Working Group, 1992), Northern Hemisphere- (Jones *et al.*, 1986a), and United States-mean temperature trends. United States-mean trend is based on gridded temperature indices. Trends in panel (d) were obtained by univariate SSA with a 15-year window.

stack spectrum represent cumulative power up to and including the last ST-PCs indicated; thus, the areas between curves are the contributions from each pair of M-SSA components indicated, 4–5, 6–7, 8–9, 10–11. In each panel, the uppermost curve is the MEM spectrum of the 'raw' series, prior to M-SSA decomposition. Notice that, in each panel, the first three M-SSA components contribute to the

lowest frequencies, whereas the other leading M-SSA components contribute to just one or two higher-frequency bands each.

The LF components (1–3) contribute most of the power in the leading ST-PC series (panel (a)) and are prominent in an area-weighted mean series (panel (b)). These largest-scale aggregations of temperature variability emphasize the LF components at the expense of higher-frequency oscillations. In grid-point spectra (panels (c)–(f)), however, the oscillatory components are nearly as strong pairwise, and stronger collectively, than the LF components. These grid-point spectra were obtained from partial reconstructions of the temperature-index series at each of four grid points. The series were obtained by first using the M-SSA form of (4) to reconstruct contributions from the ST-PCs to each S-PC (Plaut and Vautard, 1994). The reconstructed components (RCs: Ghil and Vautard, 1991; Vautard *et al.*, 1992; Dettinger *et al.*, 1995) were then projected onto their respective S-EOFs to form a time series of maps describing the temperature-index variations captured by each ST-PC in turn. Finally, grid-point series were extracted from these maps, analyzed by MEM, and the resulting spectra summed to form Figures 7(c)–(f). The same reconstructions were used to compute the area-weighted mean series of panel (b).

Reconstructing LF components 1 and 2 at all grid points yields a time series of maps showing the significant LF variations only. Differences between the combined LF patterns at five 15-year intervals during 1915–75 are shown in Figure 8 (panels (a)–(e)). LF variation of United States temperatures began (around 1915) with most of the domain cooler than the Southeastern States. The entire domain warmed until the 1940's and then cooled to minimum temperatures during the 1970's. This recent cooling was most pronounced in the Southeastern United States.

This pattern of LF warming and cooling found by M-SSA is in agreement with general patterns of warming and cooling trends of minimum and maximum temperatures during the last several decades, identified by Karl *et al.* (1993), and with changes in atmospheric circulation patterns over the Western United States indicated by recent changes in high-altitude runoff regimes (Dettinger and Cayan, 1995). Finally, this pattern can be verified by forming simple 15-year moving averages of divisional temperatures for selected states. Shown in Figure 8(f) are the moving averages for Georgia (a southeastern state), Arizona (southwestern), Idaho (northwestern), and New Hampshire (northeastern). Temperatures in Georgia have, indeed, fallen most dramatically during the period 1910–87. Note that the temperatures used in Figure 8(f) are not from the HCN data set and have not been subjected to the same corrections, filtering, or gridding as the temperature indices studied throughout this paper.

Other forms of LF variability may be present in the United States temperature series but would have been deemphasized as a result of the application of various filters prior to M-SSA. The present analysis focuses on variations that have relatively consistent expressions throughout the year and might miss trends expressed mostly in one or two seasons, with returns to a near stationary condition during the

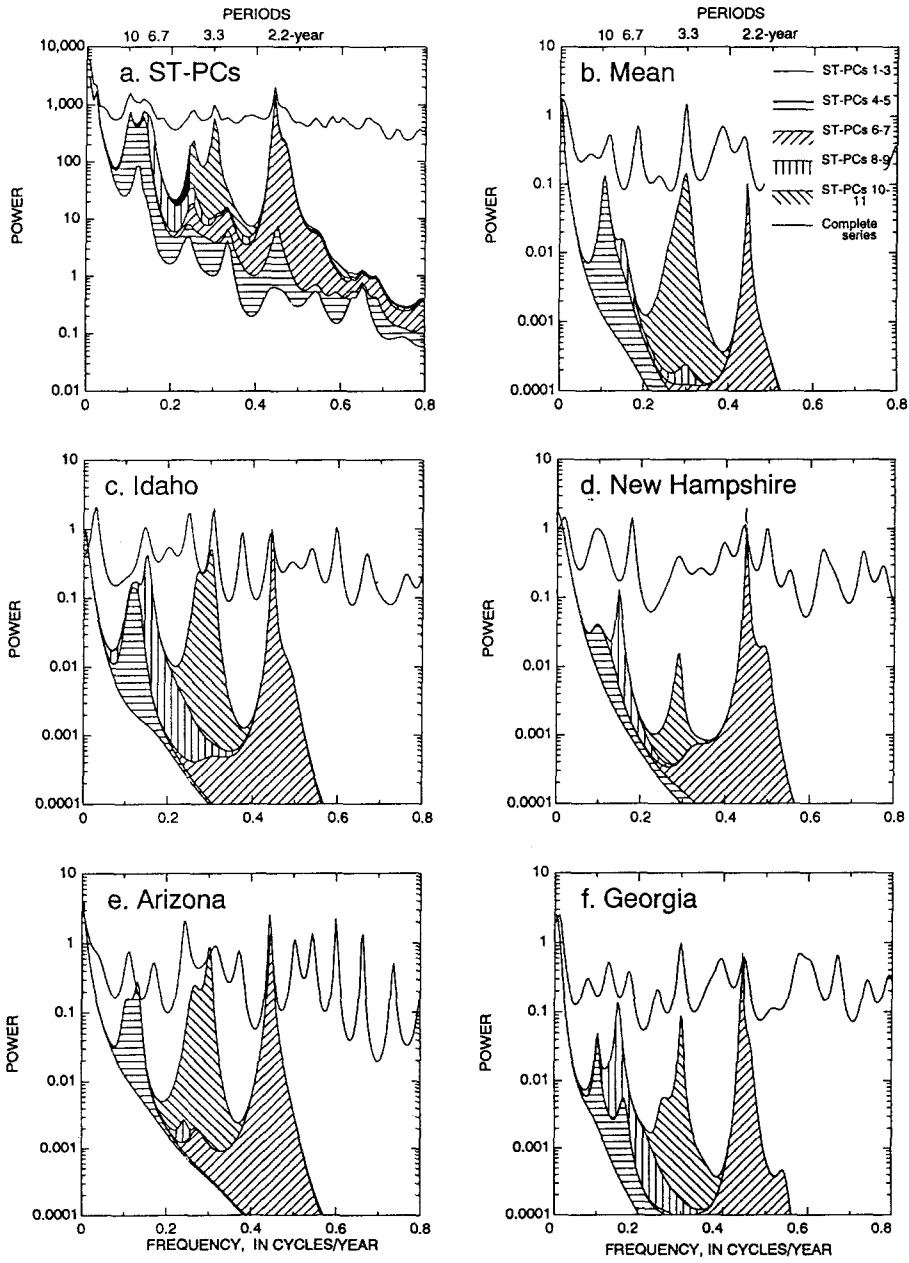

Fig. 7. Maximum-entropy stack spectra for ST-PCs 1–11 and associated reconstructions: (a) ST-PCs; (b) Area-weighted United States averages; (c) Idaho grid point (45° N 115° W); (d) New Hampshire grid point (42.5° N 72.5° W); (e) Arizona grid point (35° N 112.5° W); and (f) Georgia grid point (32.5° N 82.5° W).

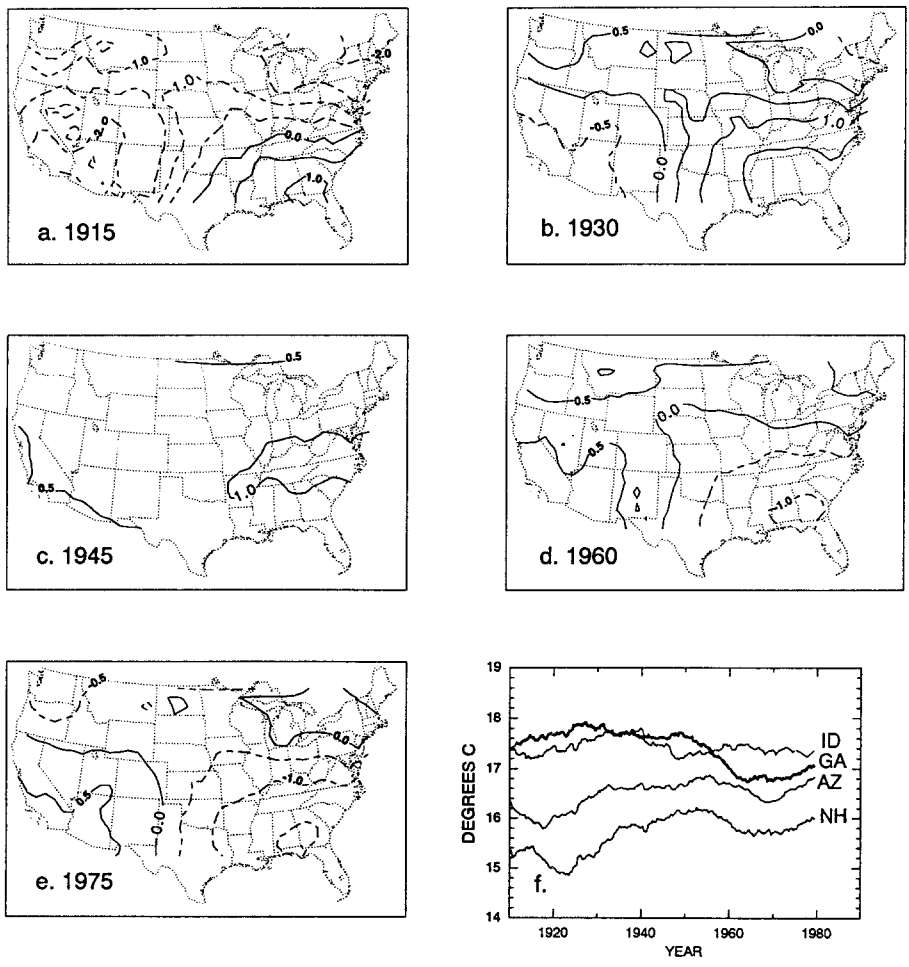

Fig. 8. Temperature-index reconstructions, times 10, from low-frequency (LF) M-SSA components 1–2 in (a) 1915; (b) 1930; (c) 1945; (d) 1960; and (e) 1975; dashed where negative; contour interval is 0.05 standard deviations (of overall variability) times 10. Panel (f) is the 15-year moving-average time series of divisional-average temperatures for Georgia (GA), Arizona (AZ), Idaho (ID) plus 10 °C, and New Hampshire (NH) plus 10 °C, based on divisional temperatures (from the National Climatic Data Center, Asheville, North Carolina).

remaining seasons. Such intermittent trends would look mostly like shorter-than-annual bursts of variability and may have been attenuated by the filters applied earlier.

4.2. INTERANNUAL OSCILLATIONS

Two strongly periodic interannual temperature oscillations, indicated by eigenvalue pairs 6–7 and 10–11, are present. The paired sixth and seventh M-SSA modes have smoothly varying ST-EOF weights for each S-PC (Figures 9(a), (b)). Notice that S-

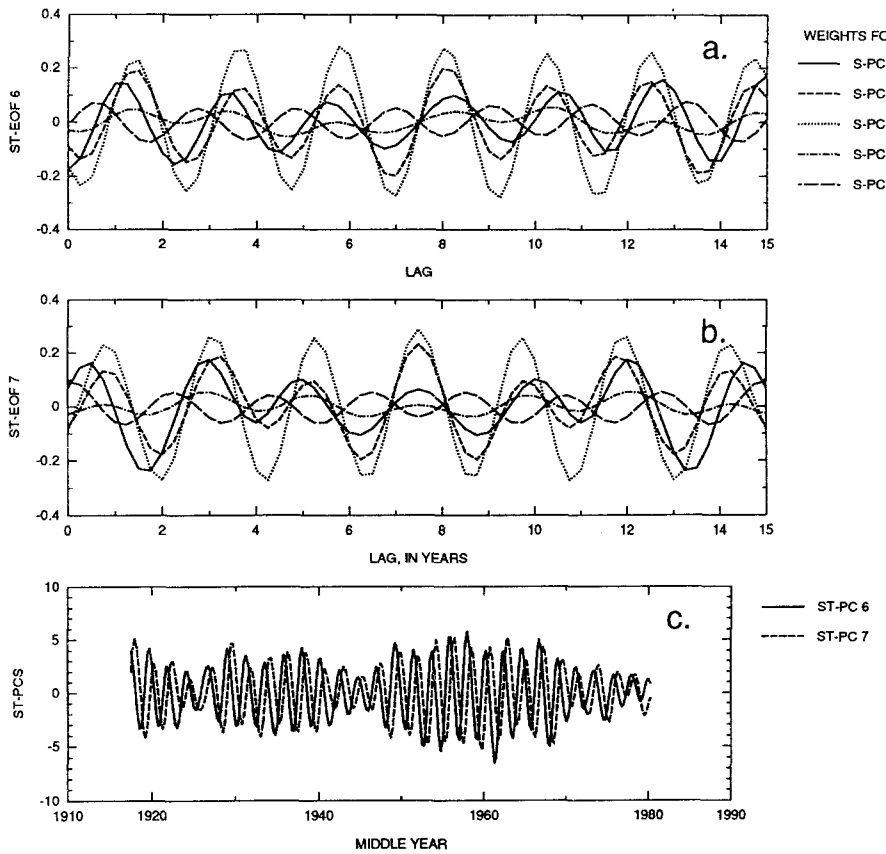

Fig. 9. ST-EOFs and ST-PCs for M-SSA components 6–7: (a) ST-EOF weights, component 6; (b) ST-EOF weights, component 7; and (c) ST-PCs for components 6 and 7.

PC 3 is weighted most strongly, followed by S-PC 2, and that the weights for these two S-PCs are in phase. Weights for S-PC 1 are near quadrature with these two, and the weights for S-PC 5 are almost opposite in phase. These phase relations indicate that S-PCs 2 and 3 lead S-PC 1, which leads S-PC 5, in this oscillation. Weights for S-PC 4 are smallest, indicating that the center-coast temperature differences are the least involved. ST-PCs 6 and 7 are clearly in quadrature (Table I and Figure 9(c)); their power spectra are indistinguishable, with a periodicity of 2.2 years (see Figure 7(a)).

This 2.2-year cycle is expressed mostly as a northeast-southwest oscillation of temperatures. For example, differences between reconstructions of selected low and high phases of ST-PC 7 are mapped in Figure 10(a). The 2.2-year oscillation, at these extremes, is characterized by temperature differences between the Northeastern and Southwestern United States. Although the pattern mapped in Figure 10(a) characterizes extremes of the oscillation, the complicated phase relationships among the ST-EOF weightings ensure that the oscillation is more complicated than

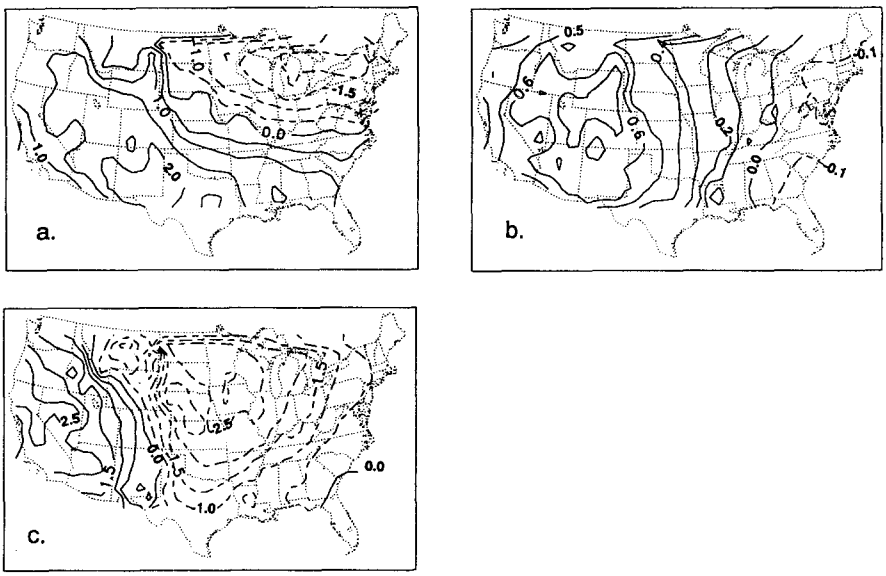

Fig. 10. Differences between opposite phases of temperature-index reconstructions from selected M-SSA components: (a) Reconstructions of ST-PC 6–7 variability at low-minus-high phases of ST-PC 7; (b) reconstructions of ST-PC 10–11 varibility at low-minus-high phases of ST-PC 10; and (c) reconstructions of ST-PC 4–5 variability at low-minus-high phases of ST-PC 5. Dashed where negative; contour intervals vary from map to map.

a simple periodic reversal of this pattern. Notice also, in Figures 7(c)–(f), that the spectral peaks associated with ST-PCs 6–7 are much stronger in the northeast and southwest (Figures 7(d), (e)) than in the northwest and southeast (Figures 7(c), (f)). This spatial pattern of 2.2-year variations corroborates the one found by Rasmusson *et al.* (1981) in a complex S-EOF analysis of temperatures band-pass filtered about 0.5 cycles/year.

The pattern in Figure 10(a) is dominated by north-south temperature differences with some east-west 'rocking'; thus, it is consistent with atmospheric-circulation patterns associated with the quasi-biennial oscillation (QBO) in NH sea-level pressure (Trenberth and Shin, 1984). The latter patterns (C1 and C2 in Trenberth and Shin) include approximately stationary centers, at about 40° latitude off both United States coasts, that fluctuate in phase opposition. The circulations associated with these centers bring warm air to the Southwest and cool air to the Northeast, and then – about 12 months later – cool air to the Southwest and warm air to the Northeast. The influence of this seesaw effect is similarly evident in a QBO component of North Atlantic sea-surface temperatures (SSTs).

The 2.2-year period also matches that of the tropical QBO, as analyzed by Rasmusson *et al.* (1990) in SSTs and surface winds and by Keppenne and Ghil (1992) in the Southern Oscillation Index (updated by Dettinger *et al.*, 1995). However, ST-PC 7 drifts into and out of phase with the QBO reconstructions of

these authors during the 78 years considered here. This is reminiscent of the lack of consistent phase relations between Trenberth and Shin's NH tropospheric QBO and the tropical stratospheric QBO or between the stratospheric and the surface QBO in the tropics (Xu, 1992). Thus, as with these other QBOs, there is no enduring phase relation between the 2.2-year cycle found here and the tropical surface QBO; direct linkages between the QBOs of the tropics and United States temperatures are difficult to infer.

ST-EOFs 10 and 11 have smoothly varying weights for S-PCs 1 and 2 (Figures 11(a) and 11(b)). The strongest weights are for S-PC 2 (east-west temperature contrasts), followed by S-PC 1 (whole-domain variations); the two S-PCs are nearly in phase. Weights for the other 3 S-PCs are weaker and less regular. ST-PCs 10 and 11 are roughly in quadrature (Table I) and each has a strong spectral peak at 3.3 years and a lesser peak at 4.0 years (Figure 7(a)). The differences between reconstructions of low and high phases of ST-PC 10 (Figure 10(b)) show that the 3.3-year oscillation corresponds to broad fluctuations of temperature in the western half of the domain, decaying from the Mississippi to the East Coast. This spatial distribution is corroborated by comparing the large 3.3-year peaks in spectra for the northwest and southwest (Figures 7(c), (e)) with the smaller peaks at eastern grid points (Figures 7(d), (f)).

The 3.3-year oscillation, although robustly present in the United States temperature data, has been reported in only a few other studies. Keppenne and Ghil (1990) identified oscillations with periods near 1.7 and 3.3 years in the pre-World War II sea-level pressures at Darwin, Australia, but these oscillations were absent from the post-war record there. Jiang *et al.* (1995) have recently shown that nonlinear ocean models of the steadily wind-driven double-gyre circulation can oscillate with a periodicity of approximately 3 years. Recent analyses of North Pacific SST and boundary-current geometries have, indeed, identified oscillations with periods near 3.3 years (Iwasaka *et al.*, 1987; Qiu and Joyce, 1992; Speich *et al.*, 1994). Perhaps the localization of the 3.3-year component of United States temperature variability within the western states is a symptom that the driving force is in the North Pacific, immediately to the west.

4.3. MID-RANGE AND DECADAL OSCILLATIONS

Eigenvalue pairs 4–5 and 8–9 correspond to less regular oscillations whose periods range from 7 to 10 years. ST-EOFs 4–5 have smoothly varying, if not quite simply periodic, weights for the various S-PCs (Figures 12(a) and 12(b)). ST-EOFs 4–5 weight S-PC 1 more than the other four, all of which are nearly in phase, and opposite to S-PC 1. The amplitudes of ST-PCs 4 and 5 (Figure 12(c)) are only intermittently large, and it is only at such times that they are in quadrature and take simple periodic forms. Their power spectra, however, are both dominated by strong peaks at 10 and 7.4 years (Figure 7(a)). Temperature variations at the extremes of the decadal oscillation (Figure 10(c)) are expressed as a seesaw between the

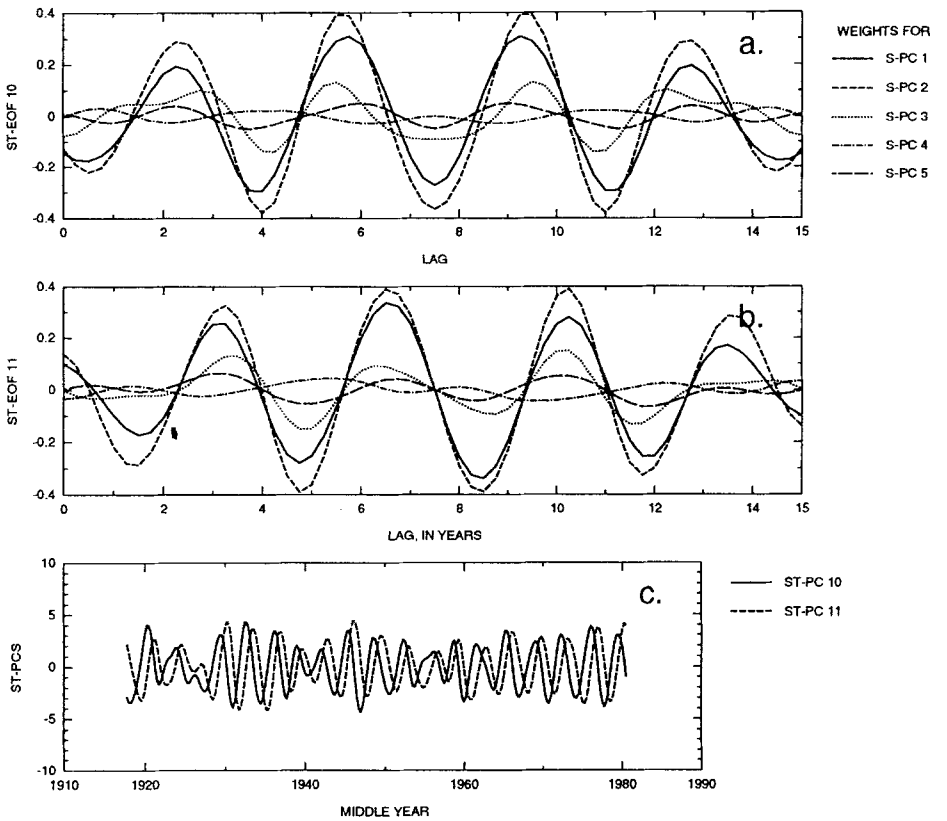

Fig. 11. ST-EOFs and ST-PCs for M-SSA components 10–11: (a) ST-EOF weights, component 10; (b) ST-EOF weights, component 11; and (c) ST-PCs for components 10 and 11.

North-Central and Western United States. In keeping with this spatial pattern, the oscillation is strongest in the western grid-point spectra (Figures 7(c), (e)) and much weaker at the eastern points (7(d), (f)). When the full oscillation is reconstructed (not shown), the transitions between Figure 10(c) and its reverse are noticeably step-like. The cycle is as strong in the United States mean series as are the two interannual oscillations (Figure 7(b)).

Oscillations with a mean period near 10 years have been reported in several studies, including Ghil and Vautard's (1991) analysis of global mean temperatures and Deser and Blackmon's (1993) analysis of North Atlantic air-sea conditions. Allen and Smith (1994) found 10-year oscillations in the global temperature and in North Equatorial Atlantic Ocean SST. Notably, the 10-year oscillations in both of these time series were quiescent from about 1920 to 1950, as are ST-PCs 4 and 5. By visual inspection, the latter, however, do not bear a consistent phase relation to the SST oscillation of Allen and Smith (1994).

The 10-year period is also close to the mean period of the sunspot-number cycle, which was 10.4 years during 1910–87, and the total length of the HCN records

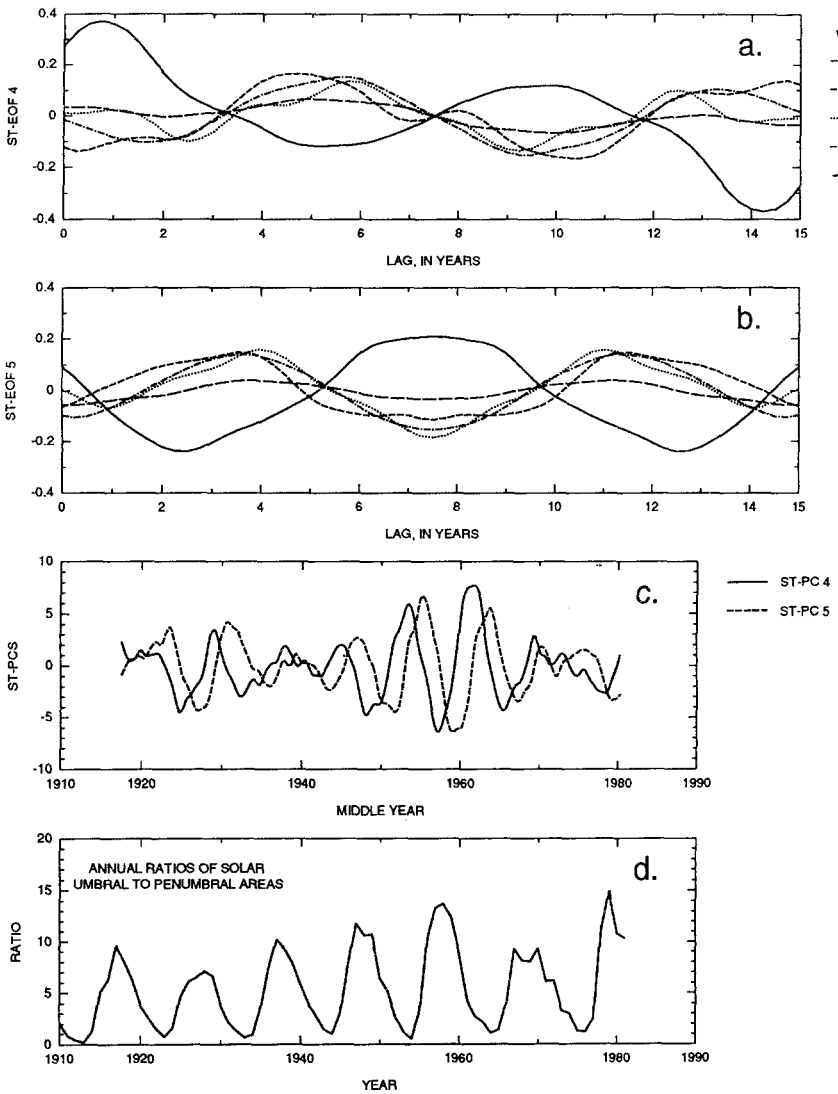

Fig. 12. ST-EOFs and ST-PCs for M-SSA components 4–5: (a) ST-EOF weights, component 4; (b) ST-EOF weights, component 5; and (c) ST-PCs for components 4 and 5; (d) Ratios of umbral-to-penumbral areas on the solar disk for the corresponding years; the umbral/penumbral ratio is a measure of the convective energy transport in the photosphere of the sun, and is therefore a measure of the sun's time-varying radiant flux (Hoyt, 1979).

analyzed here would not permit us to separate those two periods (MacDonald, 1989). The minimum amplitude of the decadal variability in ST-PCs 4 and 5 (Figure 12(c)) occurred about 10 years after the minimum in solar radiance in 1930, as indicated by umbral-to-penumbral ratios from Hoyt (1979), but the maximum of ST-PCs 4 and 5 is roughly coincident with the solar-radiance maximum near 1960 (Figure 12(d)). The differences between the sunspot-cycle and ST-PC 5

periodicities are sufficient for the two series to wander in and out of phase over the 78 years considered here, with positive ST-PC 5 sometimes coinciding with large sunspot number, and hence minimum radiance, and sometimes with small sunspot number. Our results do not indicate, therefore, a consistent relation, in phase or amplitude, between the decadal oscillation here and the sunspot cycle.

The power spectra of ST-PCs 8–9 are characterized by a strong peak at 6.7 years that is difficult to distinguish from the 7.4-year contribution of ST-PCs 4 and 5 (Figure 7(a)). Although this pair does not pass the 95% confidence tests described earlier, the isolated spectral peak present in both ST-PCs, along with previous observations of oscillations with roughly similar period, suggests that the pair may be significant. Temperature oscillations with a period of 6.2 years were identified in the IPCC global temperature record (Vautard *et al.*, 1992) and the Central England temperature record yields a period of 6.7 years (Plaut *et al.*, 1995). The spatial variability associated with ST-PCs 8–9 (not shown) is largely a reflection of S-EOF 1, the strongest signals being found in the North-Central United States and the weakest signals in the extreme West and Southwest (e.g., Figure 7(e)).

5. Summary and Discussion

In order to detect long-term climatic trends, it is necessary to analyze and understand the most reliable and extensive climate records available, both for low-frequency (LF) variability and for higher-frequency components that could complicate trend detection. To the extent possible, such analyses should represent climate variations over broad areas as well, to help with inferences on the physical mechanisms involved and to separate local variations from regional and global changes (Keppenne *et al.*, 1994). In this study, mean-monthly temperatures at 870 Historical Climatology Network (HCN) sites (Karl *et al.*, 1990) that have serially complete records for the years 1910–87 have been analyzed using an optimal-interpolation gridding scheme (Figure 1), spatial empirical-orthogonal function (S-EOF) analysis, and singular spectrum analysis (SSA). Temperature indices were interpolated onto a rectangular grid of points, 2.5° latitude and 2.5° longitude apart, and S-EOF analysis was applied in order to characterize major spatial modes of temperature variability. The time coefficients (S-PCs) of these spatial modes were adaptively filtered to remove variability that is faster than annual. Finally, the filtered S-PCs were subjected to multichannel SSA (M-SSA) with a 15-year window. M-SSA helped extract large-scale LF variability, on time scales longer than the window width, and the dominant interannual-to-decadal temperature oscillations.

The S-EOF analysis of the gridded temperature indices decomposed the temperature record into orthogonal patterns (Figure 2). The leading five patterns capture 84% of temperature-index variability; they are as follows: one that captures simultaneous variations over the contiguous United States and is weighted more

in the interior, two that capture east-west and north-south temperature contrasts, and two (possibly degenerate) patterns that capture center-coast differences and contrasts between northwest-southeast and northeast-southwest temperatures (Figure 3). Upon rotation of these S-EOFs, five dominant temperature regions were identified in the North-Central, Northwestern, Southwestern, Southeastern, and Northeastern States. Spatio-temporal variations can be described by either set of EOFs, as long as the five spatial modes are analyzed simultaneously.

M-SSA provides a means to simultaneously analyze this spatio-temporal variability. Upon application to the five leading unrotated S-EOFs, two dominant components of significant LF variability were identified, along with several leading oscillations. Together these components represent about 18% of the slower-than-annual temperature variability in the United States record. One of the leading LF modes corresponds to long-term cooling in the Southeast and warming elsewhere. The second LF mode is also expressed throughout the domain and its evolution roughly parallels Northern Hemisphere mean temperatures (Figure 6).

The leading oscillations include two distinct interannual modes, with periods of 2.2 and 3.3 years, which are very regular and persistent. The extremes of the 2.2-year interannual oscillation are characterized by temperature differences between the Northeastern and Southwestern States (Figure 10(a)). The 3.3-year cycle is present mostly in the Western States (Figure 10(b)).

Two longer-term modes that appear to be only intermittently periodic are found as well; the former exhibits 10- and 7.4-year periodicities and the latter a strong 6.7-year periodicity. The decadal oscillation is much less regular and persistent than the interannual oscillations, and it is characterized by variations that are strongest in the Central United States (Figure 10(c)).

Notably missing from the leading M-SSA components are oscillations with periods of 1.7 years and 5.4 years. As noted earlier, the tropical expression of a 3.3-year cycle seemed to be tied to a 1.7-year periodicity. Such 1.7-year periodicities also were found, together with the 3.3-year oscillation, in the unrotated S-PC 2 series (of east-west contrasts) when that series was subjected to univariate SSA. Oscillations with 5.4-year periodicities are prominent in the global mean temperature series (Ghil and Vautard, 1991) and are present in the unrotated S-PC 1 series (of whole-domain variations). Both the 1.7- and 5.4-year oscillations are strongly present in just one S-PC series each. As a consequence, they may tend to contribute less variance among the M-SSA components than do the oscillations that involve more than one S-PC, and they may have been missed in our search for the most significant spatio-temporal oscillations. Indeed, a red-noise significance test of the entire M-SSA spectrum (such as the univariate tests of Allen and Smith, 1994) might identify additional oscillations farther down among the components, but in this analysis we have focused on the dominant components only.

The dominant oscillations may be linked to the tropospheric quasi-biennial oscillations (2.2-year mode), tropical or global, to nonlinear current-system oscillations in the North Pacific (3.3-year mode), and to the solar cycle or variations in

the tropical Atlantic (10-year mode). The evidence for a connection to the QBO or to the solar cycle, as far as we can tell, is tenuous at best. Connections of the 3.3- and 10-year oscillations to the oceanic SSTs and flow patterns in the North Pacific's double-gyre circulation and the Atlantic's equatorial current system are certainly worth pursuing.

Acknowledgments

It is a pleasure to thank T. R. Karl and T. A. Boden for the HCN dataset, and members of the SSA Club (including the Toolkit makers – C. M. Strong, W. Weibel, and P. Yiou – as well as M. R. Allen and M. Kimoto) for many useful discussions. U. Lall and M. Mann read an early version of the manuscript and made constructive comments. M. D.'s work was supported at the USGS by the California District Research Program and by the Global Change Hydrology Program, and at UCLA by a UC Chancellor's Fellowship. M. G.'s research was funded by an NSF Special Creativity Award and by the U.S. Department of Energy's (DOE) National Institute for Global Environmental Change (NIGEC) through the NIGEC Western Regional Center at the University of California, Davis (DOE Cooperative Agreement No. DE-FC03-90ER61010; financial support does not constitute an endorsement by DOE of the views expressed in this article). C. K.'s research was funded at JPL by NOAA grant NA93AANAG0315.

References

Allen, M. R.: 1992, 'Interaction between the Atmosphere and Oceans on Time Scales of Weeks to Years', Ph.D. Thesis, St. Johns College, Oxford, 203 pp.

Allen, M. R. and Smith, L. A.: 1994, 'Investigating the Origins and Significance of Low-Frequency Modes of Climate Variability', *Geophys. Res. Lett.* **21**, 883–886.

Broomhead, D. S. and King, G.: 1986, 'Extracting Qualitative Dynamics from Experimental Data', *Physica D* **20**, 217–236.

Burg, J. P.: 1978, 'A New Technique for Time Series Data', in Childers, D. G. (ed.), *Modern Spectrum Analysis*, IEEE Press, New York, pp. 42–48.

Colebrook, J. M.: 1978, 'Continuous Plankton Records – Zooplankton and Environment, Northeast Atlantic and North Sea, 1948–1975', *Oceanol. Acta* **1**, 9–23.

Deser, C. and Blackmon, M. L.: 1993, 'Surface Climate Variations over the North Atlantic Ocean during Winter: 1900–1989', *J. Clim.* **6**, 1743–1753.

Dettinger, M. D. and Cayan, D. R.: 1995, 'Large-Scale Atmospheric Forcing of Recent Trends toward Early Snowmelt Runoff in California', *J. Clim.* **8**, 606–623.

Dettinger, M. D. and Ghil, M.: 1992, 'Interannual and Interdecadal Variability of Surface-Air Temperatures in the United States', *Proc., 16th Annual NOAA Climate Diagnostics Workshop*, Lake Arrowhead, Calif., 209–214.

Dettinger, M. D., Ghil, M., Strong, C. M., Weibel, W., and Yiou, P.: 1995, 'Software Expedites Singular-Spectrum Analysis of Noisy Time Series', *Eos, Trans. Am. Geophys. Union* **76**, 12, 14, 21.

Fraedrich, K.: 1986, 'Estimating the Dimensions of Weather and Climate Attractors', *J. Atmos. Sci.* **43**, 419–432.

Ghil, M. and Childress, S.: 1987, *Topics in Geophysical Fluid Dynamics: Atmospheric Dynamics, Dynamo Theory, and Climate Dynamics*, Springer-Verlag, New York, 485 pp.

Ghil, M., Halem, M., and Atlas, R., 1979, 'Time-Continuous Assimilation of Remote-Sounding Data and Its Effect on Weather Forecasting', *Mon. Wea. Rev.* **107**, 140–171.

Ghil, M. and Mo, K.: 1991a, 'Intraseasonal Oscillations in the Global Atmosphere – Part I: Northern Hemisphere and Tropics', *J. Atmos. Sci.* **48**, 752–779.

Ghil, M. and Mo, K.: 1991b, 'Intraseasonal Oscillations in the Global Atmosphere – Part II: Southern Hemisphere', *J. Atmos. Sci.* **48**, 780–790.

Ghil, M. and Vautard, R.: 1991, 'Interdecadal Oscillations and the Warming Trend in Global Temperature Time Series', *Nature* **350**, 324–327.

Guttman, L.: 1954, 'Some Necessary Conditions for Common-Factor Analysis', *Psychometrika* **19**, 146–161.

Handcock, M. S. and Wallis, J. R.: 1994, 'An Approach to Statistical Spatio-Temporal Modeling of Meteorological Fields', *J. Amer. Stat. Assoc.* **89**, 368–382.

Hoyt, D. V., 1979, 'Variations in Sunspot Structure and Climate', *Clim. Change* **2**, 79–92.

IPCC Working Group I: 1992, 'The 1992 IPCC Supplement: Scientific Assessment', in Houghton, J. T., Callander, B. A., and Varney, S. K. (eds.), *Climatic Change 1992 – The Supplementary Report to the IPCC Scientific Assessment*, Cambridge University Press, New York, pp. 1–22.

Iwasaka, N., Hanawa, K., and Toba, Y.: 1987, 'Analysis of SST Anomalies in the North Pacific and Their Relation to 500 mb Height Anomalies over the Northern Hemisphere during 1969–1979', *J. Met. Soc. Japan* **65**, 103–114.

Jiang, S., Jin, F. F., and Ghil, M.: 1995, 'Multiple Equilibria, Periodic and Aperiodic Solutions in a Wind-Driven, Double-Gyre, Shallow-Water Model', *J. Phys. Oceanogr.* **25**, 764–786.

Jones, P. D., Kelly, P. M., Goodess, G. B., and Karl, T. R.: 1986a, 'Northern Hemisphere Surface Air Temperature Variations, 1851–1984', *J. Clim. Appl. Met.* **25**, 161–179.

Jones, P. D., Raper, S. C., and Wigley, T. M.: 1986b, 'Southern Hemisphere Surface Air Temperature Variations, 1851–1984', *J. Clim. Appl. Met.* **25**, 1213–1230.

Karl, T. R.: 1988, 'Multi-Year Fluctuations of Temperature and Precipitation: The Gray Area of Climatic Change', *Clim. Change* **12**, 179–197.

Karl, T. R., Jones, P. D., Knight, R. W., Kukla, G., Plummer, N., Razuvayev, V., Gallo, K. P., Lindseay, J., Charlson, R. J., and Peterson, T. C.: 1993, 'A New Perspective on Recent Global Warming: Asymmetric Trends of Daily Maximum and Minimum Temperature', *Bull. Am. Meteor. Soc.* **74**, 1007–1023.

Karl, T. R., Koscielny, A. J., and Diaz, H. F.: 1982, 'Potential Errors in the Application of Principal Component (Eigenvector) Analysis to Geophysical Data', *J. Appl. Met.* **2**, 1183–1186.

Karl, T. R. and Quayle, R. G.: 1988, 'Climatic Change in Fact and in Theory: Are We Collecting the Facts?', *Clim. Change* **13**, 5–17.

Karl, T. R., Williams, C. N., Jr., and Quinlan, F. T.: 1990, 'United States Historical Climatology Network (HCN) Serial Temperature and Precipitation Data', Report ORNL/CDIAC-30, NDP-019/R1, Carbon Dioxide Information Analysis Center, Oak Ridge National Laboratory, Oak Ridge, Tennessee, 374 pp.

Kay, S. M.: 1988, *Modern Spectral Estimation – Theory and Application*, Prentice-Hall, Englewood Cliffs, New Jersey, 595 pp.

Keppenne, C. L., Dettinger, M. D., and Ghil, M.: 1994, 'Comment on "An Approach to Statistical Spatio-Temporal Modeling of Meteorological Fields" by Mark S. Handcock and James R. Wallis', *J. Am. Stat. Assoc.* **89**, 384–387.

Keppenne, C. L. and Ghil, M.: 1990, 'Adaptive Spectral Analysis of the Southern Oscillation Index', *Eos, Trans. Am. Geophys. Union* **71 (Supplement)**, 1227.

Keppenne, C. L. and Ghil, M.: 1992, 'Adaptive Spectral Analysis and Prediction of the Southern Oscillation Index', *J. Geophys. Res.* **97**, 20449–20554.

Keppenne, C. L. and Ghil, M.: 1993, 'Adaptive Filtering and Prediction of Noisy Multivariate Signals: An Application to Subannual Variability in Atmospheric Angular Mechanism', *Int. J. Bifurcation Chaos* **3**, 625–634.

Kimoto, M., Ghil, M., and Mo, K.: 1991, 'Spatial Structure of the 40-day Oscillation in the Northern Hemisphere Extratropics', *Proc. 8th Conf. Atmos. Oceanic Waves and Stability, Am. Met. Soc.*, 115–116.

Lau, K. M. and Chan, P. H.: 1985, 'Aspects of the 40–50 Day Oscillation during the Northern Winter as Inferred from Outgoing Longwave Radiation', *Mon. Wea. Rev.* **113**, 1889–1909.

Legates, D. R.: 1991, 'The Effect of Domain Shape on Principal Components Analyses', *Int. J. Climatol.* **11**, 135–146.

Legates, D. R.: 1993, 'The Effect of Domain Shape on Principal Components Analyses: A Reply', *Int. J. Climatol.* **13**, 219–228.

Lorenc, A. C., Bell, R. S., and MacPherson, B.: 1991, 'The Meteorological Office Analysis Correction Data Assimilation Scheme', *Quart. J. Roy. Met. Soc.* **117**, 59–90.

MacDonald, G. J.: 1989, 'Spectral Analysis of Time Series Generated by Nonlinear Processes', *Rev. Geophys.* **27**, 449–469.

Madden, R. A., Shea, D. J., Branstator, G. W., Tribbia, J. J., and Weber, R. O.: 1993, 'The Effects of Imperfect Spatial and Temporal Sampling on Estimates of the Global Mean Temperature: Experiments with Model Data', *J. Clim.* **6**, 1057–1066.

Mann, M. E. and Park, J.: 1994, 'Globally Correlated Variability in Surface Temperatures', *Proc. 6th Conf. Clim. Var., Am. Meteor. Soc.*, 297–301.

North, G. E., Bell, T. L., Cahalan, R. F., and Moeng, F. J.: 1982, 'Sampling Errors in the Estimation of Empirical Orthogonal Functions', *Mon. Wea. Rev.* **110**, 699–702.

Penland, C., Ghil, M., and Weickmann, K.: 1991, 'Adaptive Filtering and Maximum Entropy Spectra with Application to Changes in Atmospheric Angular Momentum', *J. Geophys. Res.* **96**, 22659–22671.

Penner, J. E., Dickinson, R. E., and O'Neill, C. A.: 1992, 'Effects of Aerosol for Biomass Burning on the Global Radiation Budget', *Science* **256**, 1432–1434.

Plaut, G. and Vautard, R.: 1994, 'Spells of Low-Frequency Oscillations and Weather Regimes in the Northern Hemisphere', *J. Atm. Sci.* **51**, 210–236.

Plaut, G., Ghil, M., and Vautard, R.: 1995, 'Interannual and Interdecadal Variability in 335 Years of Central England Temperatures', *Science* **268**, 710–714.

Preisendorfer, R. W.: 1988, *Principal Component Analysis in Meteorology and Oceanography*, in Mobley, C. (ed.), Elsevier Science, New York, 425 pp.

Press, W. H., Flannery, B. P., Teukolsky, S. A., and Vetterling, W. T.: 1989, *Numerical Recipes – The Art of Scientific Computing (FORTRAN Version)*, Cambridge University Press, New York, 702 pp.

Qiu, B. and Joyce, T. M.: 1992, 'Interannual Variability in the Mid- and Low-Latitude Western North Pacific', *J. Phys. Oceanogr.* **22**, 1062–1079.

Rasmusson, E. M., Arkin, P. A., Chen, W. Y., and Jalickee, J. B.: 1981, 'Biennial Variations in Surface Temperature over the United States as Revealed by Singular Decomposition', *Mon. Wea. Rev.* **109**, 587–598.

Rasmusson, E. M., Wang, X., and Ropelewski, C.: 1990, 'The Biennial Component of ENSO Variability', *J. Marine Sys.* **1**, 71–96.

Richman, M. B.: 1986, 'Rotation of Principal Components', *Int. J. Climatol.* **6**, 293–335.

Richman, M. B.: 1993, 'Comments on: "The Effect of Domain Shape on Principal Components Analyses" ', *Int. J. Climatol.* **13**, 203–218.

Speich, S., Jiang, S., Ghil, M., and Dijkstra, H. A.: 1994, 'Low-Frequency Variability of the Mid-Latitude Oceans: Numerical Experiments and Observational Evidence', *Eos, Trans. Am. Geophys. Union* **75 (Supplement)**, 90–91.

Trenberth, K. E. and Shin, W. T. K.: 1984, 'Quasi-Biennial Fluctuations in Sea Level Pressures over the Northern Hemisphere', *Mon. Wea. Rev.* **112**, 761–777.

Thomson, D. J.: 1982, 'Spectrum Estimation and Harmonic Analysis', *Proc. IEEE* **70**, 1055–1096.

Unal, Y. S. and Ghil, M.: 1995, 'Interannual and Interdecadal Oscillation Patterns in Sea Level', *Clim. Dyn.*, (in press).

Vautard, R. and Ghil, M.: 1989, 'Singular Spectrum Analysis in Nonlinear Dynamics, with Applications to Paleoclimatic Time Series', *Physica D* **35**, 395–424.

Vautard, R., Yiou, P., and Ghil, M.: 1992, 'Singular-Spectrum Analysis: A Toolkit for Short, Noisy Chaotic Signals', *Physica D* **58**, 95–126.

Watson, R. T., Rodhe, H., Oeschger, H., and Siegenthaler, U.: 1990, 'Greenhouse Gases and Aerosols', in Houghton, J. T., Jenkins, G. J., and Ephraums, J. J. (eds.), *Climate Change – The IPCC Scientific Assessment*, Cambridge University Press, New York, pp. 1–40.

Weare, B. C. and Nasstrom, J. S.: 1982, 'Examples of Extended Empirical Orthogonal Function Analysis', *Mon. Wea. Rev.* **110**, 481–485.

Wigley, T. M. L. and Barnett, T. P.: 1990, 'Detection of the Greenhouse Effect in the Observations', in Houghton, J. T., Jenkins, G. J., and Ephraums, J. J. (eds.), *Climate Change – The IPCC Scientific Assessment*, Cambridge University Press, New York, pp. 241–255.

Xu, J.-S.: 1992, 'On the Relationship between the Stratospheric QBO and the Tropospheric SO', *J. Atmos. Sci.* **49**, 725–734.

Yamamoto, R. and Hoshiai, M.: 1980, 'Recent Change of the Northern Hemisphere Mean Surface Air Temperature Estimated by Optimum Interpolation', *Mon. Wea. Rev.* **107**, 1239–1244.

(Received 12 September, 1994; in revised form 15 May, 1995)